Oxide nanoparticles in an Al-alloyed oxide dispersion strengthened steel: crystallographic structure and interface with ferrite matrix

Zhang, Zhenbo; Pantleon, Wolfgang

Published in:
Philosophical Magazine

Link to article, DOI:
10.1080/14786435.2017.1316876

Publication date:
2017

Document Version
Peer reviewed version

Oxide nanoparticles in an Al-alloyed oxide dispersion strengthened steel: crystallographic structure and interface with ferrite matrix

Zhenbo Zhang[1*], Wolfgang Pantleon[2]

[1]*School of Materials, University of Manchester, Manchester, M13 9PL, UK*

[2]*Section of Materials and Surface Engineering, Department of Mechanical Engineering, Technical University of Denmark, 2800 Kgs. Lyngby, Denmark*

*Corresponding author (Z.B Zhang)

E-mail: zhenbo.zhang@manchester.ac.uk; zbzhang85@gmail.com

Oxide nanoparticles in an Al-alloyed oxide dispersion strengthened steel: crystallographic structure and interface with ferrite matrix

Oxide nanoparticles are quintessential for ensuring the extraordinary properties of oxide dispersion strengthened (ODS) steels. In this study, the crystallographic structure of oxide nanoparticles, and their interface with the ferritic steel matrix in an Al-alloyed ODS steel, i.e. PM2000, were systematically investigated by high resolution transmission electron microscopy. The majority of oxide nanoparticles were identified to be orthorhombic $YAlO_3$. During hot consolidation and extrusion, they develop a coherent interface and a near cuboid-on-cube orientation relationship with the ferrite matrix in the material. After annealing at 1200 °C for 1 hour, however, the orientation relationship between the oxide nanoparticles and the matrix becomes arbitrary, and their interface mostly incoherent. Annealing at 1300 °C leads to considerable coarsening of oxide nanoparticles, and a new orientation relationship of pseudo-cube-on-cube between oxide nanoparticles and ferrite matrix develops. The reason for the developing interfaces and orientation relationships between oxide nanoparticles and ferrite matrix under different conditions is discussed.

Key words: oxide dispersion strengthened steel; oxide nanoparticles; crystallographic structure; interface; orientation relationship

Introduction

Oxide-dispersion-strengthened (ODS) steels are considered as structural materials for next-generation fission and fusion reactors because of their excellent resistance to both irradiation damage and high-temperature creep [1, 2]. Such extraordinary physical and mechanical properties originate from thermally quite stable nanoscale oxide dispersoids [1], and hence investigations on oxide nanoparticles is one of the main focus of ODS steels. In the last decade, extensive research has been carried out to determine the crystallographic structure of oxide nanoparticles, and their interface and orientation relationships with the ferritic (i.e. body centred cubic) steel matrix in various ODS steels [3-6].

ODS steels can be categorized into two main groups based on the chemical constituents of the oxide dispersoids: (i) Al-alloyed ODS steels, such as MA956 [7, 8] or PM2000 [9]; and (ii) Ti-alloyed ODS steels without Al, such as MA957 [7, 8], ODS EUROFER [10] or 14YWT [3]. Among these ODS steels, in particular high Cr- and Al-alloyed ODS ferritic steels are promising candidate cladding materials for nuclear fission reactors due to their better corrosion resistance against lead-bismuth eutectic coolants [11-13]. Compared to Ti-alloyed ODS steels, the oxide nanoparticles in Al-alloyed ODS steels are much less understood. Fabrication of ODS steels involves a sequence of decomposition of yttria during ball milling, and re-precipitation of yttrium oxide during hot consolidation and subsequent processing [14]. Since Al has a high affinity to oxygen [15], the re-precipitated oxide nanoparticles are no longer pure yttria. They have been determined to be yttrium-aluminum oxides by Electron Energy Loss Spectroscopy (EELS) [16] and Electron Dispersive X-Ray Spectroscopy (EDS) [17-19]. But there are at least four different yttrium aluminum oxides known in the Y-Al-O system [20], namely $Y_4Al_2O_9$ (yttrium-aluminum-monoclinic, YAM), $YAlO_3$ (yttrium-aluminum-hexagonal, YAH), $YAlO_3$ (yttrium-aluminum-perovskite, YAP) and $Y_3Al_5O_{12}$ (yttrium-aluminum-garnet, YAG). These possible variants complicate the identification of the oxide nanoparticles in Al-alloyed ODS ferrtic steels and their relationships with the ferrite matrix [16, 17, 21-26]. Using EELS technique, Kimenkov et al. [16] found that the oxide dispersoids in a Fe-20Cr-5Al ODS steel are mainly composed of YAG and YAP. However, in a similar ODS Fe-Cr-Al steel (MA956), the majority of oxide nanoparticles were identified as YAM by high resolution transmission electron microscopy (HRTEM) [5]. Recent studies by Dou et al. [23, 26] have shown that, in their Al-alloyed ODS steel, both YAH and YAP exist, and the fraction of YAH increases with a decreasing in consolidation temperature. In summary, the interface and

orientation relationships between the oxide nanoparticles and the ferrite matrix are reported with very large discrepancies. In addition, the evolution of the interface and orientation relationships during annealing of ODS steels is relevant, since any changes in these aspects may alter their irradiation performance. To the authors' knowledge, these issues have not been thoroughly investigated for Al-alloyed ODS steels yet.

In this study, the oxide nanoparticles in the ODS Fe-Cr-Al alloy PM2000 were investigated systematically by HRTEM, with respect to the crystal structure of the oxide nanoparticles, the interface and orientation relationships between the oxide nanoparticles and the ferrite matrix. Firstly, the crystal structure and the nanoparticle/matrix interface were identified in the as received material, i.e. PM2000 after hot consolidation. Then the thermal stability of the oxide nanoparticles and the evolution of their interface with the ferrite matrix were examined in samples annealed at high temperatures for different periods. Such systematic analysis provided solid evidence of the character of oxide nanoparticles in PM2000 and the potential changes during processing or service at high temperatures, which are not only of scientific importance but also of technological significance in terms of understanding and improving the performance of this material during application at high temperature.

Experimental

PM2000 was received in the form of a hot-extruded rod with a diameter of 13 mm. It was produced by Plansee GmbH, Reutte, Austria, following the procedure of mechanical milling and hot-extrusion described in [9]. The nominal chemical composition of PM2000 is shown in Table 1.

The crystallographic structure of the oxide nanoparticles was characterized by HRTEM. As the oxide nanoparticles are embedded in the ferrite matrix, it is difficult to obtain

clear imaging and electron diffraction of the oxide particles exclusively. To eliminate the disturbing interference when identifying the crystal structure of oxide nanoparticles due to the strong channelling effect of the ferrite matrix, oxide nanoparticles were extracted by means of carbon replica. Characterization of the interface and orientation relationship between the oxide nanoparticles and the ferrite matrix was conducted on TEM foils, which were prepared by twin jet electropolishing followed by a cleaning process by ion milling. Electropolishing was carried out in a solution of ethanol (70 vol. %), water (12 vol. %), 2-butoxy-ethanol (10 vol. %), and perchloric acid (8 vol. %) at -20 °C. Further argon ion polishing was performed on a Gatan PIPS II operating at 4 keV with a gun angle of ±3°. The oxide nanoparticles in samples annealed at 1200 °C for 1 hour, and 1300 °C for 1 hour, 10 hours and 100 hours were also characterized. To avoid oxidation at high temperatures, PM2000 samples were annealed in a high vacuum furnace with Ar atmosphere. All TEM characterizations were carried out using a JEOL 3000F field emission gun transmission electron microscope operating at 300 kV with a double tilt holder (+/- 25°). TEM images and HRTEM images were acquired by a couple charged device camera; the point resolution of the microscope being about 0.17 nm. The software CaRine Crystallography 3.1 was used to construct the crystal structure of oxide particles and simulate their diffraction patterns.

Results

Structure of oxide nanoparticles

The bright field TEM image in Fig. 1a shows the typical features and distribution of oxide nanoparticles in the as-received PM2000. The oxide particles are well-dispersed in the ferritic matrix with almost equiaxed shape and large size variation.. The distribution of the Feret diameters (calliper diameters) for 1196 randomly selected oxide

particles is shown in Fig. 1b. The mean diameter of the oxide nanoparticles is 14.2 nm with a standard deviation of the distribution (STDEV) of 10.0 nm. These findings are quite consistent with the result reported by other researchers on the same material [18].

The crystallographic structure of oxide nanoparticles extracted by carbon replica from the PM2000 sample was characterized by HRTEM. Fast Fourier Transformation (FFT) patterns of the HRTEM images were obtained and all of them were compared with simulated diffraction patterns of the four possible yttrium-aluminum oxides, namely YAM, YAG, YAP and YAH. About 30 oxide nanoparticles with various orientations to the incident electron beam located in different regions were examined, and all of them were identified as orthorhombic $YAlO_3$ (YAP), with space group of Pnma (group no. 206), and lattice parameters a=5.330 Å, b=7.375 Å and c=5.180 Å. Fig. 2 shows examples of HRTEM images and corresponding FFT patterns for three oxide nanoparticles. The crystalline lattice of these oxide nanoparticles can be clearly identified from the HRTEM images. The incident electron beams are along the [101], [111] and [012] zone axes for Fig. 2a, b, and c, respectively. The unit cell structure of the YAP and the electron diffraction patterns along the above three zone axes, as obtained by CaRIne Crystallography 3.1, are shown in Fig. 3. It is evident that the simulated patterns (Fig. 3b-d) and the FFT patterns of the HRTEM images (Fig. 2) are in very good agreement.

It should be mentioned that a small amount of quite large particles were identified both in the current study and previous reports [17, 19]. These large particles were found to be alumina and titanium carbonitrides. Due to their very low number fraction (less than 1%) and very large sizes (normally above 100 nm), they play only a minor role in strengthening and enhancing the irradiation tolerance of the ODS steel. Thus they are

not taken into consideration as nanoparticles in this study.

Orientation relationship between oxide nanoparticles and ferrite matrix in the as-received material

To obtain the orientation relationship between YAP and the ferrite (α) matrix, HRTEM characterization was conducted on conventional thin foils. Systematic characterizations were done, and HRTEM images of three oxide nanoparticles and the ferrite matrix are shown in Fig. 4. The three YAP nanoparticles were inspected along different zone axes, with the incident electron beam along three directions, namely [110], [221], [112]. It is seen from the HRTEM images that all the particles have coherent lattices with the surrounding matrix. Their corresponding FFT patterns reveal that for all three particles, the parallel and coherent planes of YAP and ferrite are $(220)_{YAP}$ and $(110)_{\alpha}$, respectively. This orientation relationship develops mainly because ferrite and YAP have very close lattice spacings for these crystallographic planes, with 2.12 Å for the $(110)_{\alpha}$,, and 2.24 Å, and 2.21 Å for the $(220)_{YAP}$, and $(022)_{YAP}$ planes, respectively.

Since YAP and ferrite have very different crystallographic symmetry with a cuboid and a cube as unit cell respectively, the above orientation relationship might not be very obvious when viewing along other directions of YAP. With regard to the coherent plane, $(220)_{YAP}$ plane has only one other crystallographic equivalent plane, i.e. $(2\bar{2}0)_{YAP}$. If slight deviations are allowed, two more planes ($(022)_{YAP}$, $(0\bar{2}2)_{YAP}$) can be considered to be almost equivalent, whereas ferrite has six equivalent {110} planes. Besides, the angles between the individual $\{220\}_{YAP}$ planes are slightly different from that of $\{110\}_{\alpha}$. Therefore, when one set of $\{220\}_{YAP}$ plane is parallel to a certain $\{110\}_{\alpha}$ plane, the others of the $\{110\}_{\alpha}$ and $\{220\}_{YAP}$ planes are not exactly parallel. This issue

can be more clearly illustrated in the reciprocal space, by the reciprocal lattice points of YAP and ferrite along the [111] zone axis, where all six equivalent {110} planes are visible. It can be seen from Fig. 5 that $(\bar{1}10)_\alpha \| (0\bar{2}2)_{YAP}$ and $(1\bar{1}0)_\alpha \| (02\bar{2})_{YAP,}$ but other $\{110\}_\alpha$ and $\{220\}_{YAP}$ planes are not parallel. Therefore, if the observed {110} plane of ferrite is neither $(\bar{1}10)_\alpha$, nor $(1\bar{1}0)_\alpha$, no coherency will be observed. Two examples are shown in the HRTEM images in Fig. 6.

In Fig. 6a, {110} lattice planes of ferrite are imaged clearly (incident electron beam nearly along $\langle 111\rangle_\alpha$), and Moiré fringes appear in the oxide particle, which implies the existence of a semi-coherent relationship between YAP and ferrite. The diffraction spots of $(1\bar{2}1)_{YAP}$ and $(01\bar{1})_\alpha$ are indexed in the corresponding FFT pattern. It can be derived from the FFT pattern that $(1\bar{2}1)_{YAP}$ is not exactly parallel to $(01\bar{1})_\alpha$, but there is rotation of a few degrees between them. This can be rationalized by the reciprocal pattern (Fig. 6) where $(1\bar{2}1)_{YAP}$ and $(01\bar{1})_\alpha$ appear simultaneously, because of the relaxed Bragg condition for electron diffraction in TEM. Due to the fact that the lattice spacings of $(1\bar{2}1)_{YAP}$ and $(01\bar{1})_\alpha$ are quite different (2.62 Å and 2.12 Å, respectively), Moiré fringes appear caused by double diffraction from the two individual sets of planes [27]. To validate the suggested indexing based on the interference of superimposed channelling effects of particle and matrix, a quantitative interpretation of the Moiré fringes is added. When the orientation relationship between particle and surrounding matrix gives rise to overlap of two gratings with different periodicities d_1 and d_2, parallel Moiré fringes at their interface will emerge with a periodicity [28]

$$D_{Moiré} = \frac{d_1 d_2}{|d_2 - d_1|} \qquad (1)$$

The spacing of Moiré fringes $D_{\text{Moiré}}$ measured on the particle in Fig. 6a is 9.76 Å. With d_1 being the spacing of $(110)_\alpha$, the spacing d_2 is found from Eq. (1) to be either 2.64 Å or 1.72 Å for $d_2>d_1$ or $d_2<d_1$,respectively. Comparing with the lattice parameters of YAP, only the former value is consistent with a YAP plane spacing (2.62 Å), corresponding to the $(1\bar{2}1)_{\text{YAP}}$ planes. This is indeed what has been found as Miller index for the involved YAP planes from the FFT pattern.

Another example of the orientation relationship between oxide nanoparticle and ferrite matrix is shown in Fig. 6b, in which the incident electron beam is nearly along the $[111]_{\text{YAP}}$. In this case, Moiré patterns emerge at the YAP particle interface as well. $(110)_\alpha$ is nearly parallel to $(022)_{\text{YAP}}$, and $(011)_\alpha$ is nearly parallel to $(220)_{\text{YAP}}$. As a quite large mismatch between $(101)_\alpha$ and $(202)_{\text{YAP}}$ exists, Moiré fringes emerge due to the different periodicities (2.12 Å and 1.86 Å, respectively) of these two individual gratings. Consistency between the measured and calculated (based on Eq. (1)) periodicity of Moiré fringes (15.77 Å) demonstrates the correctness of the indexing.

From the findings of Fig. 4 and Fig. 6 that $(\bar{1}10)_\alpha \| (0\bar{2}2)_{\text{YAP}}$ and $(1\bar{1}0)_\alpha \| (02\bar{2})_{\text{YAP}}$ as illustrated in Fig. 5, it can be concluded that approximately a cuboid-on-cube orientation relationship between YAP nanoparticles and the ferrite matrix develops in the as received PM2000. Due to the different symmetry of orthorhombic and cubic lattices, interfacial coherency is differently observed along different directions, especially as relaxation of the Bragg condition is considered in the TEM imaging. A schematic diagram illustrating the observed orientation relationship is shown in Fig. 7.

The unit cells of YAP and ferrite are shown as cuboid and cube, respectively, with lengths proportional to their lattice parameters. Due to the difference in crystalline symmetry between YAP and ferrite, the $(110)_{\alpha}$ and $(220)_{YAP}$ planes are not exactly parallel when aligning $\boldsymbol{a}_{YAP}||\boldsymbol{a}_{\alpha}$, $\boldsymbol{b}_{YAP}||\boldsymbol{b}_{\alpha}$ and $\boldsymbol{c}_{YAP}||\boldsymbol{c}_{\alpha}$. A rotation about 9.1° around the $\boldsymbol{c}_{YAP}$ axis is necessary to make $(110)_{\alpha}$ and $(220)_{YAP}$ parallel; this process is illustrated in Fig. 7d. After rotating 9.1° around $\boldsymbol{c}_{YAP,}$ the orientation relationship between YAP is $(110)_{\alpha}||(220)_{YAP}$ and $[001]_{\alpha}||[001]_{YAP}$ and the $[111]_{YAP}$ and $[111]_{\alpha}$ have an angle of 5.6°, which is consistent with the observation in Fig. 6. This orientation relationship can be expressed equivalently as $\boldsymbol{c}_{YAP}||\boldsymbol{c}_{\alpha}$, whilst $\angle(\boldsymbol{a}_{YAP},\boldsymbol{a}_{\alpha})=9.1°$ and $\angle(\boldsymbol{b}_{YAP},\boldsymbol{b}_{\alpha})=9.1°$.

Thermal stability of oxide nanoparticles

The thermal stability of the oxide nanoparticles in ODS steels is important to maintain the mechanical properties and irradiation tolerance of the material at elevated temperatures. Fig. 8 shows the Feret diameter distribution of oxide nanoparticles measured in the TEM foils of PM2000 after annealing at 1200 °C and 1300 °C, respectively. It is seen that after annealing at 1200 °C for 1 hour, the mean size of oxide nanoparticles does not increase significantly compared to that prior to annealing (14.2 nm). Substantial coarsening happened when the material was annealed at 1300 °C. The average diameters of the oxide nanoparticles increases to 18.5 nm, 24.7 nm and 27.9 nm during annealing at 1300 °C for 1 hour, 10 hours and 100 hours, respectively. It is also evident from the size distributions that the fraction of oxide nanoparticles with sizes smaller than 10 nm is largely reduced after annealing for 10 hours and 100 hours.

Orientation relationship between oxide nanoparticles and ferrite matrix after annealing

Annealing at 1200 °C

Fig. 9 shows HRTEM images and corresponding FFT patterns and Inverse Fast Fourier Transformation (IFFT) images of two YAP nanoparticles in the sample after annealing at 1200 °C for 1 hour. In Fig. 9a, the incident electron beam is along $[100]_{\alpha}$ and $[112]_{YAP}$, and the FFT pattern of this HRTEM image is indexed accordingly. It can be seen that $(110)_{\alpha}$ and $(02\bar{1})_{YAP}$ are almost parallel, and $(1\bar{1}0)_{\alpha}$ planes form an angle of 5° with $(2\bar{2}0)_{YAP}$ planes. However, the lattice spacing of $(02\bar{1})_{YAP}$ is 2.90 Å, while the lattice spacing of $(110)_{\alpha}$ is 2.12 Å. Due to such a large difference in spacing, the interface cannot remain coherent and misfit dislocations are expected at the interface. After filtering the background noise and selecting the diffraction signal from $(02\bar{1})_{YAP}$, and $(1\bar{1}0)_{\alpha}$ and $(110)_{\alpha}$, an IFFT image was constructed. This IFFT image clearly reveals periodical misfit dislocations around the YAP/ferrite interface with a periodicity of 7.61 Å. The distance between misfit dislocations

$$D_{misfit} = \frac{(d_2 + d_1)^2}{4|d_2 - d_1|} \qquad (2)$$

can also be calculated [28] when two gratings with different periodicities d_1 and d_2 are superimposed. With the values $d_{(02\bar{1})YAP}$ and $d_{(110)Fe}$, a value for D_{misfit} of 7.62 Å can be derived from Eq. (2), which is quite consistent with the measured value.

Fig. 9b presents another example of the YAP/ferrite interface of a sample annealed at 1200 °C for 1 hour. As this YAP nanoparticle is on the edge of the TEM thin foil with

part of it outside the ferrite matrix, the diffraction patterns of oxide and matrix can be obtained separately, and therefore the orientation relationship between YAP and ferrite can be derived easily. It is seen that the incident electron beam is along the $[100]_{\alpha}$ and $[210]_{YAP}$, and that after indexing the FFT patterns no clear orientation relationship between them can be concluded. Furthermore, based on the superimposed region in the HRTEM image, no evidence for any coherent interface can be gained.

Another typical feature of the YAP nanoparticles after annealing at 1200 °C for 1 hour is shown in Fig. 10. Moiré fringes are frequently observed on the interface of YAP and ferrite. As seen from the HRTEM image and the corresponding FFT pattern (Fig. 10a), the incident electron beam is along a $[100]_{\alpha}$, and clear Moiré fringes appear at the interface of YAP and ferrite due to double diffraction. The visible plane of YAP under this condition is the $(202)_{YAP}$ plane, which forms an angle of 19.1° with the $(110)_{\alpha}$ plane. It is these two sets of planes with a rotation angle between them that leads to the formation of Moiré fringes when superimposed. To verify this claim, a simple simulation (Fig. 10b) is performed by overlaying two sets of parallel gratings after a relative rotation of 19.1°, which are the counterparts of the planes of $(202)_{YAP}$ and $(110)_{\alpha}$. The apparent Moiré pattern is in very good agreement with the observed HRTEM image, with respect to both, the direction and the spacing of the Moiré fringes. Therefore, it seems evident that these Moiré fringes originate from double diffraction of $(202)_{YAP}$ and $(110)_{\alpha}$.

More than 20 oxide nanoparticles were examined, and none of them showed a coherent interface with ferritic matrix. Hence, it is concluded that the initial cuboid-on-cube orientation relationship vanishes after annealing at 1200 °C for 1 hour; the orientation relationship between YAP nanoparticles and ferrite matrix becomes arbitrary and no

coherency between them is preserved.

Annealing at 1300 °C

HRTEM images and corresponding FFT patterns of three YAP nanoparticles with diameters between 12 nm to 25 nm from the sample annealed at 1300 °C for 10 hours are shown in Fig. 11. It is evident from the HRTEM images that the YAP particles have clear facets, which is quite different from the spherical YAP particles in the as-received condition.. All facets in these three examples show consistent alignment with one of two specific types of crystallographic planes of ferrite, namely either $\{110\}_{\alpha}$ or $\{200\}_{\alpha}$. Periodical diffraction patterns, which are supposed to originate from double diffraction of YAP and ferrite, with lower intensity, but higher frequency than that of ferrite can be seen in the FFT patterns parallel to either $\{110\}_{\alpha}$ or $\{200\}_{\alpha}$.

By masking the double diffraction patterns as well as the patterns from the ferrite matrix, an IFFT image could be constructed after filtering the noise background. In the obtained IFFT images shown in Fig. 12, the smaller dots correspond to the atomic planes of $\{100\}_{\alpha}$, whereas the larger dots are caused by double diffraction of superimposed $\{010\}_{\alpha}$ and $\{010\}_{YAP}$.

A sketch motivating the formation of such an image is presented in Fig. 13. As described in section 3.4.1, when two gratings with different periodicities d_1 and d_2 are superposed, Moiré fringes emerge if the Bragg diffraction condition for the operating reflection is closely satisfied. As illustrated in Fig. 13 the two gratings representing the lattice planes of $(110)_{\alpha}$ and $(200)_{YAP}$ are parallel and overlap along the horizontal direction, and those of $(1\bar{1}0)_{\alpha}$ and $(002)_{YAP}$ are parallel and overlapping as well along the vertical direction. Because double diffraction takes place in two non-parallel

directions, Moiré patterns with periodical dots can be observed in the image plane [29]. This is why periodical dots appear in Fig. 12 instead of fringes. Due to the difference between the lattice spacing $d_{(101)\alpha}$ and $d_{(200)YAP}$ with $5d_{(101)\alpha} \approx 4d_{(200)YAP}$, matching planes are every fifth $(101)_\alpha$ and every fourth $(200)_{YAP}$ or $(002)_{YAP}$, which is also observed as the periodicity of the Moiré patterns. These predicted patterns are very similar to that observed in Fig. 12. Accordingly, the orientation relationship between the YAP particles and the ferrite matrix can be described as $(110)_\alpha \| (200)_{YAP}$ or $(110)_\alpha \| (002)_{YAP}$, and $[100]_\alpha \| [202]_{YAP}$. More than 20 oxide nanoparticles were examined; all of them were facetted and showed this orientation relationship which was not observed in PM2000 prior to annealing.

Discussion

Identification of the oxide nanoparticles in PM2000

The crystal structure of the oxide nanoparticles in PM2000 has been identified as orthorhombic $YAlO_3$ (yttrium-aluminium-perovskite, YAP) by systematic HRTEM studies. Solid evidence has been gathered from the HRTEM images and the full agreement between their FFT patterns with simulated diffraction patterns of YAP. Taking advantage of the carbon replica extraction approach, any interference caused by ferrite matrix has been totally excluded when indexing the oxide particles. Nevertheless, one should be cautious about the process of carbon replica extraction of oxide nanoparticles, because the etchant (Nital solution) applied to reveal the oxide particles may react with the oxide particles during the process and thereby inducing artificial products. Nevertheless, very consistent results on the crystal structure of oxide nanoparticles were obtained in this study between particles both in TEM foils and carbon replicas. This confirms the validity of the indexing results for the oxide

nanoparticles in carbon replicas.

Previous studies on the characterization of oxide nanoparticles in Al-alloyed ODS steels have presented controversial results: It is generally accepted that the formation of oxide dispersoids involves fragmentation of Y_2O_3 particles, decomposition of Y_2O_3 fragments during ball milling, and re-precipitation of oxide nanoparticles during the consolidation process [14, 30]. YAP and YAH are the most frequently reported Y-Al-O nanoparticles in Al-alloyed ODS steel. However, YAH is thought to be an unstable product and would transform to YAP at elevated temperatures [26]; this is probably the reason for not finding YAH in PM2000. YAG was also claimed to be identified in PM2000 [17, 18], however, no solid evidence about the crystal structure was provided in these reports, and the HRTEM image in the report was wrongly indexed due to designating an erroneous zone axis [17]. YAM was only determined in Al-alloyed ODS steel by Hsiung et al. [21, 25], but since YAM is only thought to be formed at very high temperatures, one cannot expect to find this oxide in PM2000. Hence, it is concluded that YAP is the dominant oxide nanoparticles in PM2000.

It is noteworthy that the lattice parameters of YAP has a relationship of $a \approx c$ and $b \approx \sqrt{2}a$. Therefore, a pseudo-cubic lattice can be used as an alternative to describe the structure of orthorhombic YAP. In this manner, it becomes more straightforward to compare YAP with other cubic materials, and to describe, for instance, the orientation relationship of YAP with ferrite, which has a cubic structure. A sketch of the unit cells (cuboids) of the orthorhombic primitive crystalline lattice of YAP and the corresponding unit cell (cube) of the pseudo-cubic lattice is shown in Fig. 4 as thin and thick lines, respectively. Some important correspondences of crystallographic directions between the orthorhombic and the pseudo-cubic lattice are: $[100]=½[101]_{pc}$,

$[101]=[001]_{pc}$, $[110]=½[121]_{pc}$ and $[010]=[010]_{pc}$, as illustrated in Fig. 14.

Interface and orientation relationship between oxide nanoparticles and ferrite matrix

When a second phase particle is precipitated, the interface of the particle/matrix can be classified as either coherent, semi-coherent, or incoherent. In the hot consolidated state, coherent interfaces are observed between the YAP nanoparticles and the ferrite matrix in PM2000. This is proved by HRTEM imaging along the different crystallographic directions of YAP. As the interfacial energy of a coherent particle is lower than an incoherent one (interphase boundary energy for coherent interfaces ranges from 5 to 200 mJ/m^2, while for incoherent interphases are between 800 and 2500 mJ/m^2 [28]), the nucleation of coherent precipitates is favored, if the lattice mismatch between particles and matrix on certain planes is small causing only minor elastic distortions. After annealing at 1200 °C for 1 hour, however, an incoherent interface is observed and orientation relationship between YAP and ferrite becomes arbitrary. This loss of coherency is suggested to be caused by changes in the ferrite matrix during annealing.

Upon annealing at 1200 °C, the driving force from the stored energy after hot-extrusion is sufficient to enable recovery of the deformation structure and formation of recrystallization nuclei. Thus, recrystallization of the ferrite matrix occurs in PM2000. Fig. 15 shows the microstructure of the as-received sample and the sample annealed at 1200 °C for 1 hour. The orientation maps obtained by EBSD demonstrate that the grain structure coarsened significantly during annealing with the average grain size increasing from 1.1 μm to about 5 mm. As a consequence of sweeping recrystallization fronts, the orientation of the majority of the initial ferrite matrix is expected to change after being consumed by recrystallizing grains. On the other hand, the diameter of oxide

nanoparticles (as shown in Fig. 8a) does not change appreciably during annealing. As the oxide nanoparticles are geometrically constricted by the surrounding matrix and unable to reorient during the recrystallization process, the initial cuboid-on-cube orientation relationship between oxide nanoparticles and ferrite will be lost and replaced by an arbitrary relationship as the recrystallizing ferrite grains grow around the oxide nanoparticles. Semi-coherent and incoherent interfaces are therefore frequently observed, as shown in Fig. 9 and Fig. 10.

During annealing at 1300 °C, a new orientation relationship between YAP and ferrite developed. A sketch illustrating the change in the orientation relationship between YAP and ferrite due to annealing at 1300 °C is presented in Fig. 16. The orientation relationship between a YAP nanoparticle and ferrite in the as-received sample is near cuboid-on-cube, with $(110)_{\alpha}||(220)_{YAP}$ and $\langle 001\rangle_{\alpha}||\langle 001\rangle_{YAP}$, as illustrated in the Fig. 16a. The orientation relationship changes to $(110)_{\alpha}||(200)_{YAP}$ and $\langle 100\rangle_{\alpha}||\langle 202\rangle_{YAP}$ after annealing at 1300 °C for 10 hours. It is seen from the diagram in Fig. 16b that this new orientation relationship can be achieved by rotating the unit cell of ferrite along the direction ***b*** by about 45°, while maintaining the initial orientation of the YAP unit cell. This newly developed orientation relationship can be expressed in another straightforward way when describing YAP with its pseudo-cubic lattice. In this manner, the orientation relationship between ferrite and the pseudo-cubic lattice of YAP (YAP_{pc}) in the sample after annealing at 1300 °C for 10 hours can be specified as $(110)_{\alpha}||(202)_{YAPpc}$, and $[100]_{\alpha}||[200]_{YAPpc}$ and hence described as pseudo cube-on cube relationship.

The reorientation of YAP nanoparticles is suggested to be driven by minimizing the interfacial energy. At 1300 °C, the ferrite matrix is coarsened by recrystallization

(similar to annealing at 1200 °C) and most of YAP nanoparticles must have lost their coherency with the matrix. Due to the high energy of an incoherent interface, YAP nanoparticles are prone to reorient to reduce the interfacial energy. As significant growth of the YAP nanoparticles occurs during annealing at 1300 °C, the geometrical constrains which suppressed reorientation at 1200 °C are released and the YAP nanoparticles may reorient to lower the interfacial energy while growing larger. The developing particle morphology is a result of a balance between the compositional interface energy and the misfit elastic strain energy of the elastic distortion fields [31-33]. The faceted shape developing for the YAP nanoparticles in the ferrite matrix indicates that the elastic energy is predominant [34]. All facets correspond very consistently to low-indexed crystallographic planes, along either $(101)_{YAP}$ or $(100)_{YAP}$ planes, corresponding to $(100)_{\alpha}$ or $(110)_{\alpha}$, respectively. Therefore, the formation of facets of low energy is seen as part of the driving force for reorientation.

Conclusions

The crystallographic structure of oxide nanoparticles in the Al-alloyed ferritic ODS steelPM2000 was characterized thoroughly by HRTEM. The interfaces and orientation relationships between oxide nanoparticles and ferrite matrix were determined in the as-received and annealed conditions. The most important findings can be summarized as follows:

(1) The majority of oxide nanoparticles in PM2000 are identified to be orthorhombic $YAlO_3$ (yttrium-aluminium-perovskite, YAP).
(2) In the as-received state (after consolidation and hot-extrusion), the YAP nanoparticles show a coherent interface with ferrite matrix and a near cuboid-on-cube orientation relationship.

(3) No change in the size of YAP nanoparticles was observed after annealing at 1200 °C for 1 hour, whereas considerable coarsening happens when annealing at 1300 °C for 1 hour or more.

(4) Due to recrystallization of the ferrite matrix during annealing at 1200 °C for 1 hour, the orientation relationship between YAP and ferrite becomes arbitrary and the initial coherency lost.

(5) After annealing at 1300 °C for 10 hours, the orientation relationship between YAP and ferrite changed into a pseudo-cube-on-cube relationship. Clearly faceted shapes of YAP are observed after annealing, with facets parallel to either $\{100\}_\alpha$ or $\{110\}_\alpha$.

Acknowledgement

Financial support from the Sino-Danish Center for Education and Research is gratefully acknowledged.

Reference

[1] G.R. Odette, M.J. Alinger, and B.D. Wirth, *Recent developments in irradiation-resistant steels*, Annu. Rev. Mater. Res., 38 (2008), pp. 471-503.

[2] I. Chant, and K.L. Murty, *Structural materials issues for the next generation fission reactors*, JOM 62 (2010), pp. 67-74.

[3] A. Hirata, T. Fujita, Y.R. Wen, J.H. Schneibel, C.T. Liu, and M.W. Chen, *Atomic structure of nanoclusters in oxide-dispersion-strengthened steels*, Nat. Mater. 10 (2011), pp. 922-926.

[4] M.K. Miller, D.T. Hoelzer, E.A. Kenik, and K.F. Russell, *Stability of ferritic MA/ODS alloys at high temperatures*, Intermetallics 13 (2005), pp. 387-392.

[5] L.L. Hsiung, M.J. Fluss, S.J. Tumey, B.W. Choi, Y. Serruys, F. Willaime, and A. Kimura, *Formation mechanism and the role of nanoparticles in Fe-Cr ODS steels developed for radiation tolerance*, Phys. Rev. B 82 (2010), pp. 184103-13.

[6] J. Ribis, and Y. de Carlan, *Interfacial strained structure and orientation relationships of the nanosized oxide particles deduced from elasticity-driven*

morphology in oxide dispersion strengthened materials, Acta Mater. 60 (2012), pp. 238-252.

[7] T.S. Chou, and H. Bhadeshia, *Crystallographic texture in mechanically alloyed oxide dispersion-strengthened MA956 and MA957 steels*, Metall. Trans. A 24 (1993), pp. 773-779.

[8] T.S. Chou, and H. Bhadeshia, *Recrystallization temperatures in mechanically alloyed oxide-dispersion-strengthened MA956 and MA957 steels*, Mater. Sci. Eng. A 189 (1994), pp. 229-233.

[9] C. Capdevila, and H. Bhadeshia, *Manufacturing and microstructural evolution of mechanuically alloyed oxide dispersion strengthened superalloys*, Adv. Eng. Mater. 3 (2001), pp. 647-656.

[10] C.A. Williams, E.A. Marquis, A. Cerezo, and G.D.W. Smith, *Nanoscale characterisation of ODS-Eurofer 97 steel: An atom-probe tomography study*, J. Nucl. Mater. 400 (2010), pp. 37-45.

[11] P. Hosemann, H.T. Thau, A.L. Johnson, S.A. Maloy, and N. Li, *Corrosion of ODS steels in lead-bismuth eutectic*, J. Nucl. Mater. 373 (2008), pp. 246-253.

[12] S. Takaya, T. Furukawa, K. Aoto, G. Muller, A. Weisenburger, A. Heinzel, M. Inoue, T. Okuda, F. Abe, S. Ohnuki, T. Fujisawa, and A. Kimura, *Corrosion behavior of Al-alloying high Cr-ODS steels in lead-bismuth eutectic*, J. Nucl. Mater. 386-88 (2009), pp. 507-510.

[13] S. Takaya, T. Furukawa, M. Inoue, T. Fujisawa, T. Okuda, F. Abe, S. Ohnuki, and A. Kimura, *Corrosion resistance of Al-alloying high Cr-ODS steels in stagnant lead-bismuth*, J. Nucl. Mater. 398 (2010), pp. 132-138.

[14] M.J. Alinger, G.R. Odette, and D.T. Hoelzer, *On the role of alloy composition and processing parameters in nanocluster formation and dispersion strengthening in nanostuctured ferritic alloys*, Acta Mater. 57 (2009), pp. 392-406.

[15] L.S. Darken, and R.W. Gurry, *Physical chemistry of metals*, McGraw-Hill, New York, 1953.

[16] M. Klimenkov, A. Moslang, and R. Lindau, *EELS analysis of complex precipitates in PM 2000 steel*, Eur. Phys. J-Appl. Phys. 42 (2008), pp. 293-303.

[17] M. Klimiankou, R. Lindau, A. Moslang, and J. Schroder, *TEM study of PM2000 steel*, Powder Metall. 48 (2005), pp. 277-287.

[18] P. Krautwasser, A. Czyrska-Filemonowicz, M. Widera, and F. Carsughi, *Thermal stability of dispersoids in ferritic oxide-dispersion-strengthened alloys*, Mater. Sci. Eng. A 177 (1994), pp. 199-208.

[19] Y.Z. Shen, T.T. Zou, S. Zhang, and L.Z. Sheng, I*dentification of Oxide Phases in Oxide Dispersion Strengthened PM2000 Steel*, ISIJ Int. 53 (2013), pp. 304-310.

[20] O. Fabrichnaya, H.J. Seifert, T. Ludwig, F. Aldinger, and A. Navrotsky, *The assessment of thermodynamic parameters in the Al2O3-Y2O3 system and phase relations in the Y-Al-O system*, Scand. J. Metall. 30 (2001), pp. 175-183.

[21] L.L. Hsiung, M.J. Fluss, and A. Kimura, *Structure of oxide nanoparticles in Fe-16Cr MA/ODS ferritic steel*, Mater. Lett. 64 (2010), pp. 1782-1785.

[22] J.H. Lee, and J.H. Kim, *Characterization of Oxide Nanoparticles in Al-Free and Al-Containing Oxide Dispersion Strengthened Ferritic Steels*, J. Nanosci. Nanotechno. 13 (2013), pp. 6169-6173.

[23] P. Dou, A. Kimura, R. Kasada, T. Okuda, M. Inoue, S. Ukai, S. Ohnuki, T. Fujisawa, and F. Abe, *TEM and HRTEM study of oxide particles in an Al-alloyed high-Cr oxide dispersion strengthened steel with Zr addition*, J. Nucl. Mater. 444 (2014), pp. 441-453.

[24] C.H. Zhang, A. Kimura, R. Kasada, J. Jang, H. Kishimoto, and Y.T. Yang, *Characterization of the oxide particles in Al-added high-Cr ODS ferritic steels*, J Nucl. Mater. 417 (2011), pp. 221-224.

[25] L.L. Hsiung, M.J. Fluss, S.J. Tumey, B.W. Choi, Y. Serruys, F. Willaime, and A. Kimura, *Formation mechanism and the role of nanoparticles in Fe-Cr ODS steels developed for radiation tolerance*, Phys. Rev. B 82 (2010), pp. 1-13

[26] P. Dou, A. Kimura, T. Okuda, M. Inoue, S. Ukai, S. Ohnuki, T. Fujisawa, and F. Abe, *Polymorphic and coherency transition of Y-Al complex oxide particles with extrusion temperature in an Al-alloyed high-Cr oxide dispersion strengthened ferritic steel*, Acta Mater. 59 (2011), pp. 992-1002.

[27] D.B. Williams, and C.B. Carter, *Transmission Electron Microscopy: A Textbook for Materials Science*, Springer, 2009.

[28] J.M. Howe, *Interfaces in materials: atomic structure, thermodynamics and kinetics of solid-vapor, solid-liquid and solid-solid interfaces*, Wiley, 1997.

[29] K. Creath, and J.C. Wyant, *Moire and fringe projection techniques, in Optical Shop Testing, 2nd Edition*, D. Malacara ed., Wiley, New York, 1992.

[30] M.J. Alinger, *On the formation and stability of nanometer scale precipitates in ferritic alloys during processing and high temperature service*, PhD thesis. Univ. Calif., Santa Barbara (2004).

[31] P.W. Voorhees, G.B. Mcfadden, and W.C. Johnson, *On the Morphological Development of 2nd-Phase Particles in Elastically-Stressed Solids*, Acta Metall. 40 (1992), pp. 2979-2992.

[32] A. Maheshwari, and A.J. Ardell, *Morphological Evolution of Coherent Misfitting Precipitates in Anisotropic Elastic Media*, Phys. Rev. Lett. 70 (1993), pp. 2305-2308.

[33] A.J. Ardell, and Nicholso.Rb, *On Modulated Structure of Aged Ni-Al Alloys*, Acta Metall. 14 (1966), pp. 1295-1309.

[34] S. Onaka, N. Kobayashi, T. Fujii, and M. Kato, *Energy analysis with a superspherical shape approximation on the spherical to cubical shape transitions of coherent precipitates in cubic materials*, Mater. Sci. Eng. A 347 (2003), pp. 42-49.

Table 1 Nominal chemical composition (wt. %) of PM2000.

Cr	Al	Ti	Y_2O_3	C	Fe
20	5.5	0.5	0.5	0.02	Bal.

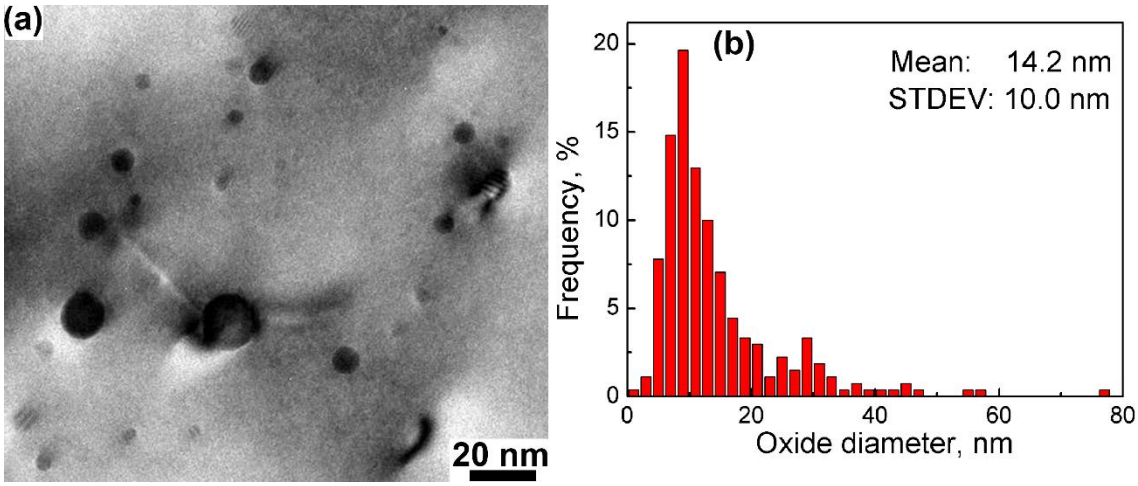

Figure 1. Bright field TEM image from the longitudinal section of the as-received PM2000 showing the dispersed oxide nanoparticles, and (b) distribution of Feret diameters of 1196 oxide nanoparticles measured from a number of TEM images.

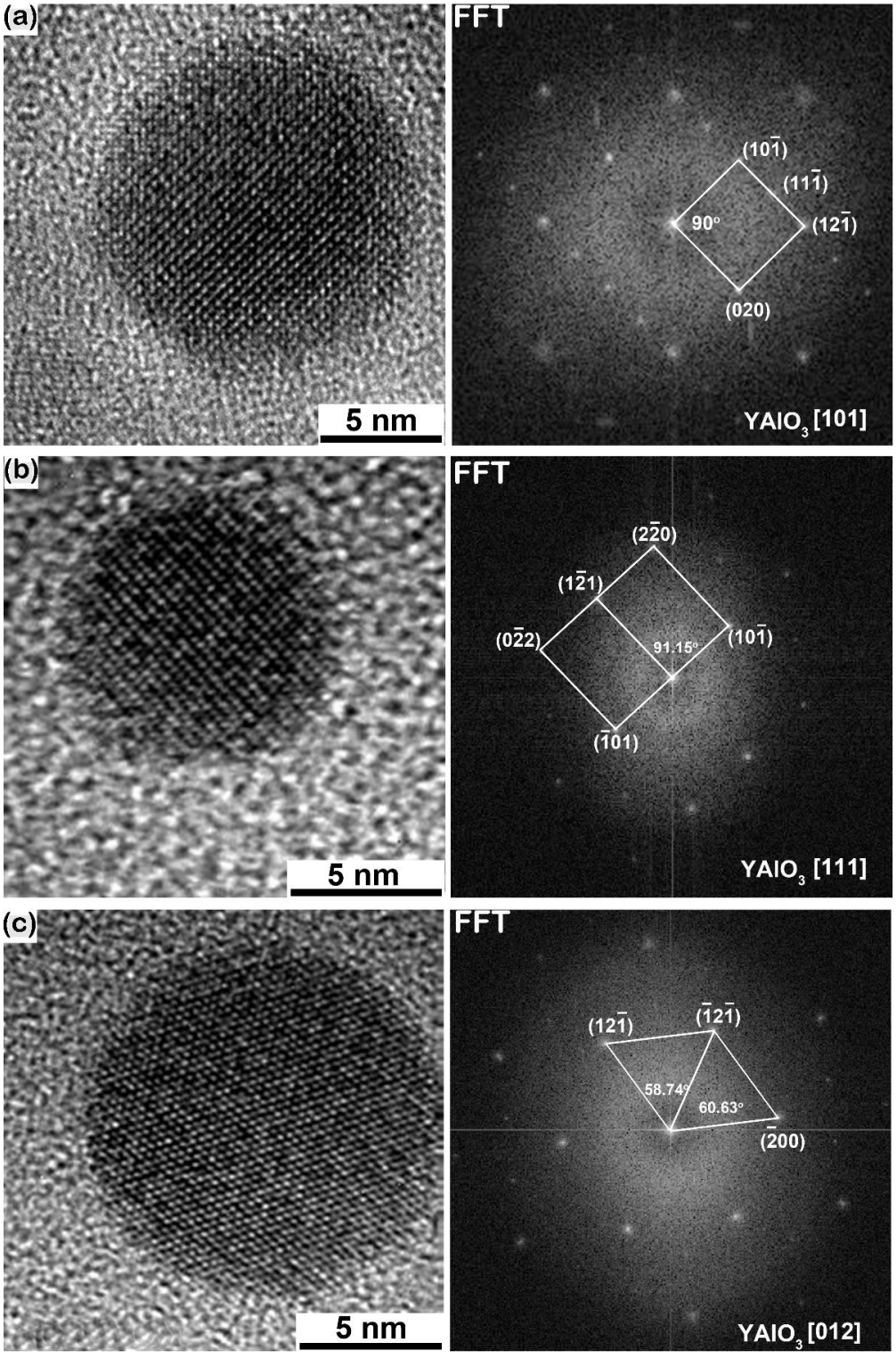

Figure 2. HRTEM images and their corresponding FFT patterns of oxide nanoparticles extracted by carbon replicas from as-received PM2000 with incident electron beam along different zone axes of the oxide nanoparticles. By indexing the FFT patterns, the direction of incident electron beam is determined to be along (a) [101], (b) [111] and (c) [012] zone axis of $YAlO_3$.

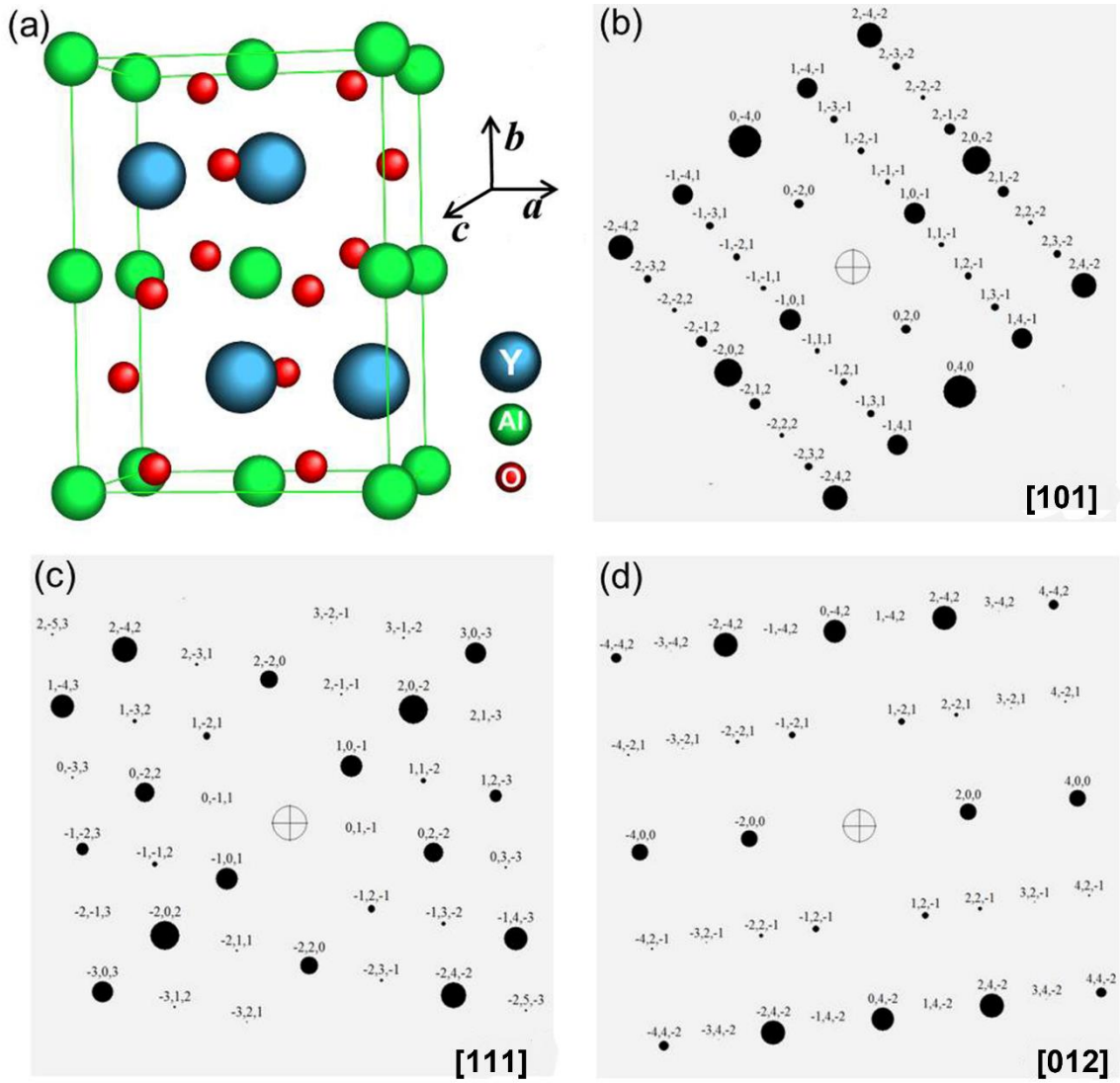

Figure 3. (a) Schematic representation of the orthorhombic unit cell of $YAlO_3$ (forming a cuboid) and the simulated diffraction patterns along different zone axes (b) [101], (c) [111] and (d) [012]. The simulated patterns are rotated to match the FFT patterns in Fig. 2 (a), (b), and (c), respectively. (CaRIne Crystallography 3.1 was used to construct the unit cell structure and simulate the diffraction patterns).

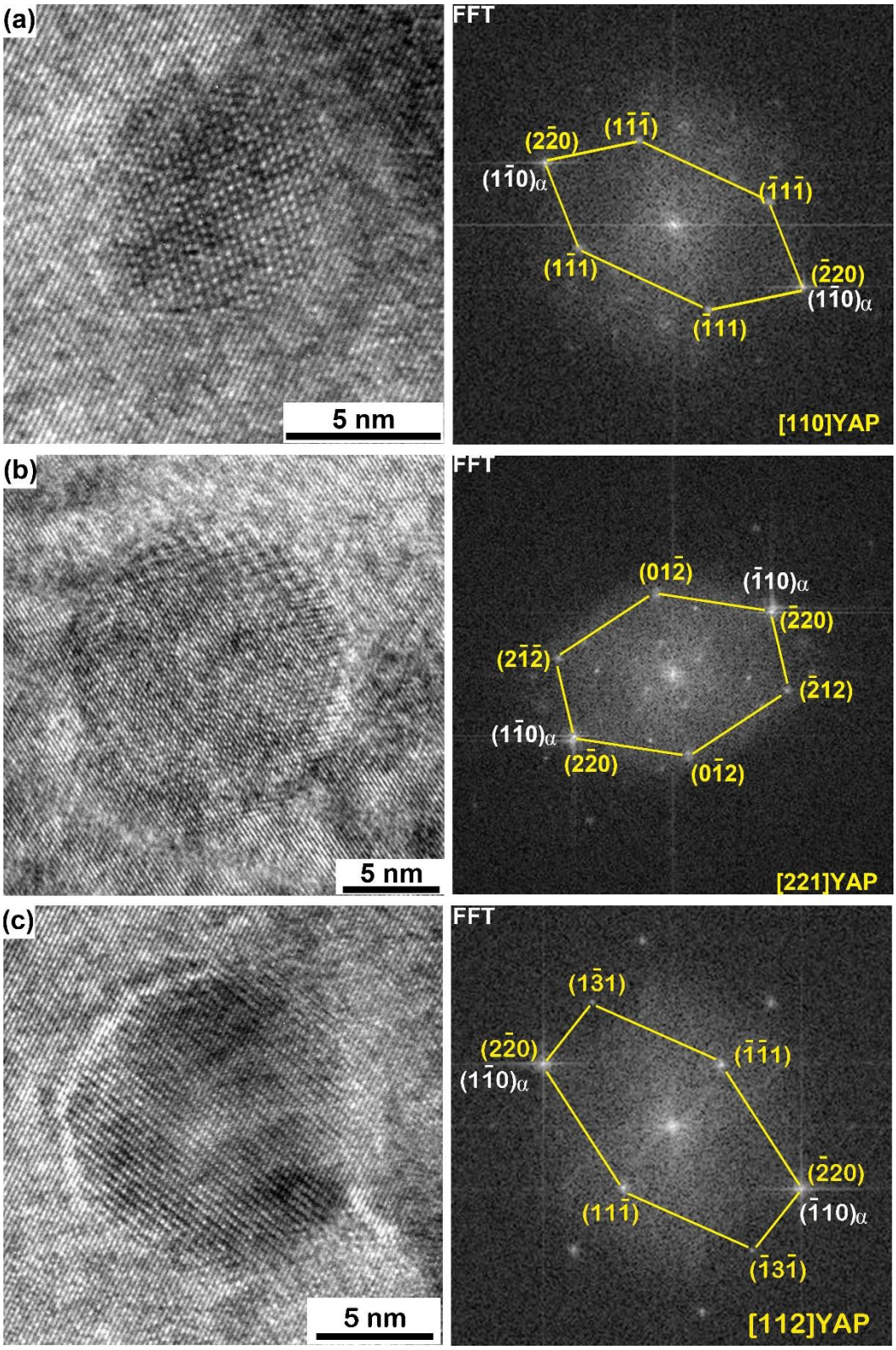

Figure 4. HRTEM images of as-received PM2000 and the corresponding FFT patterns showing three YAP particles, with the electron beam along different zone axes of YAP, (a) [110], (b) [221], and (c) [112], showing lattice coherency with the ferrite matrix.

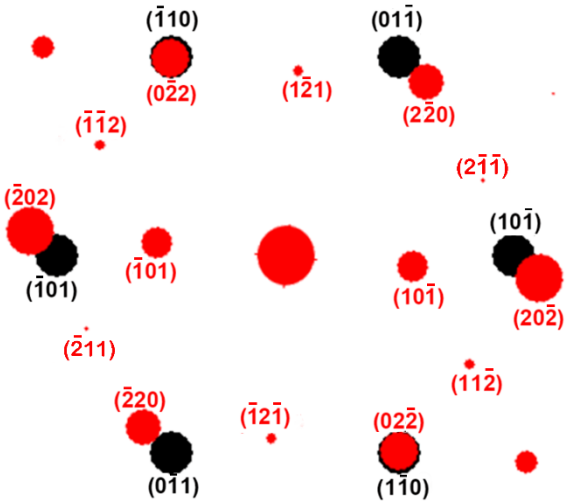

Figure 5. Simulated diffraction patterns of YAP (dots and plane designations in red) and ferrite (dots and plane designations in black) along the [111] zone axis for both.

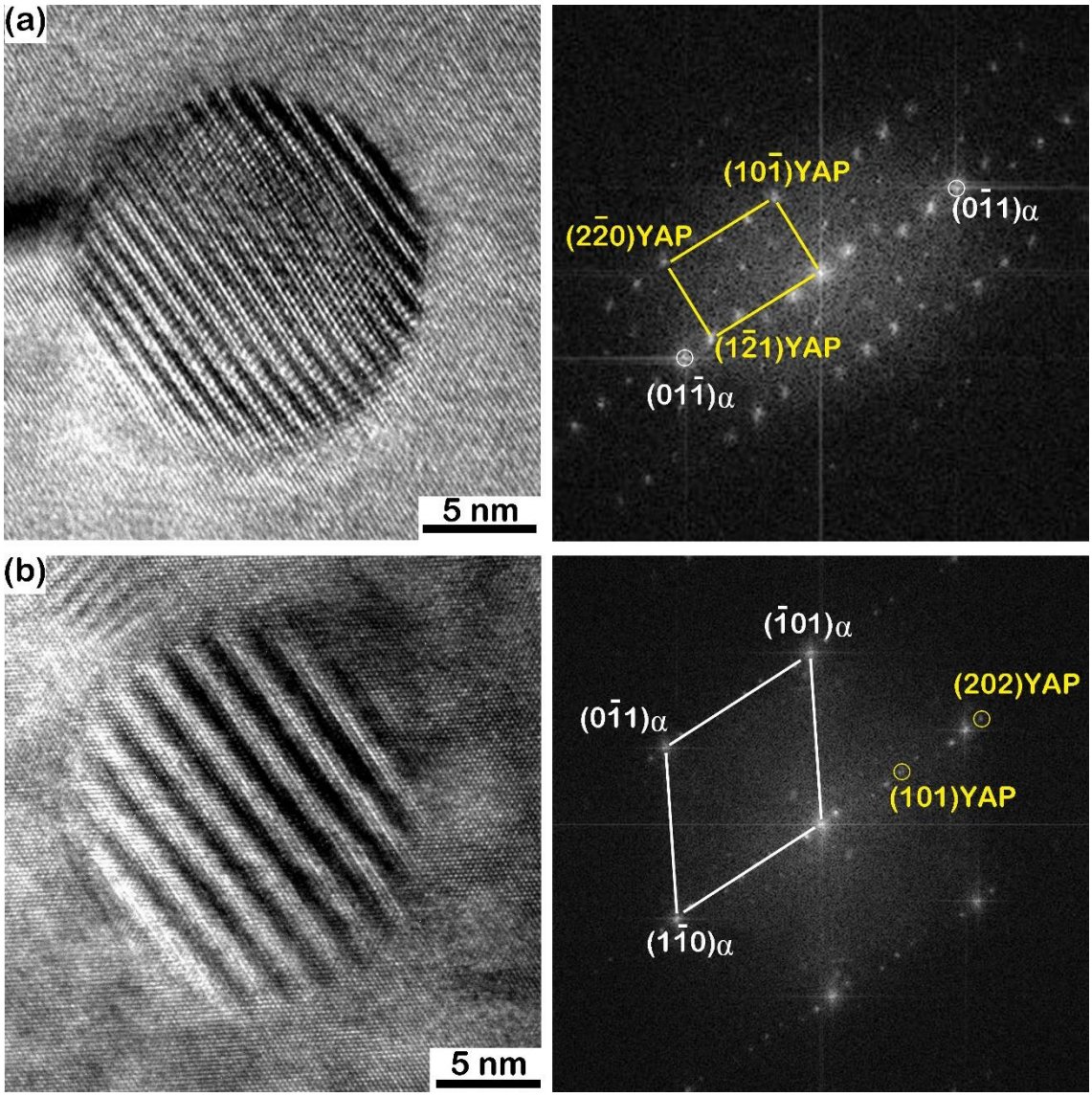

Figure 6. HRTEM images and the corresponding FFT patterns showing two different YAP particles and the ferrite matrix, with the incident electron beam along different zone axes, (a) $[111]_{\alpha}$ and near $[111]_{YAP}$, (b) $[111]_{YAP}$ and near $[111]_{\alpha}$.

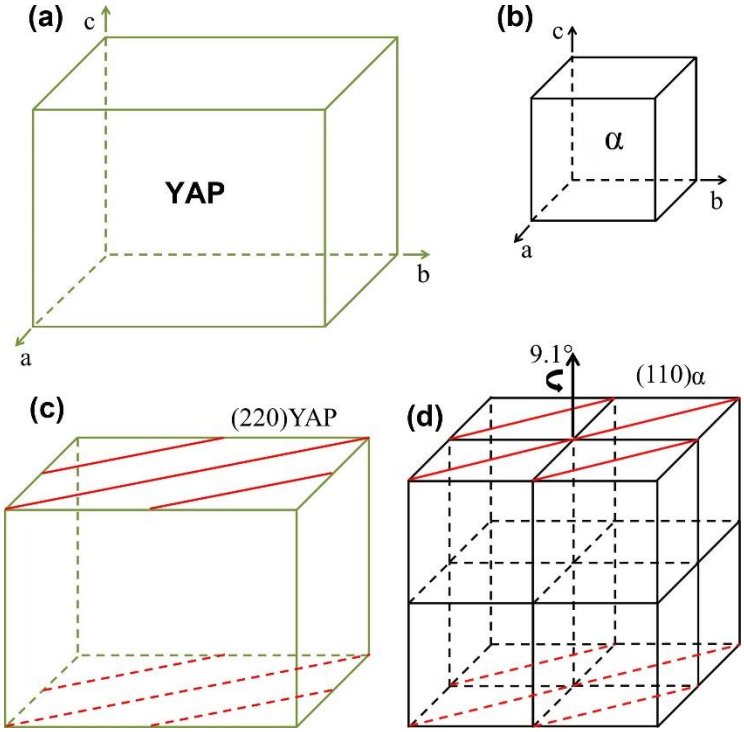

Figure 7. Sketches showing the orientation relationship between the YAP nanoparticle and the ferrite matrix in PM2000: (a) unit cell of YAP (cuboid), (b) unit cell of ferrite (cube), (c) unit cell of YAP with (220) plane traces shown in red lines, (d) eight unit cells of ferrite with (110) plane traces shown as red lines. The crystal of ferrite must be rotated 9.1° along ***c***, resulting in an angle of 9.1° between $\boldsymbol{a}_{\mathrm{YAP}}$ and $\boldsymbol{a}_{\alpha}$.

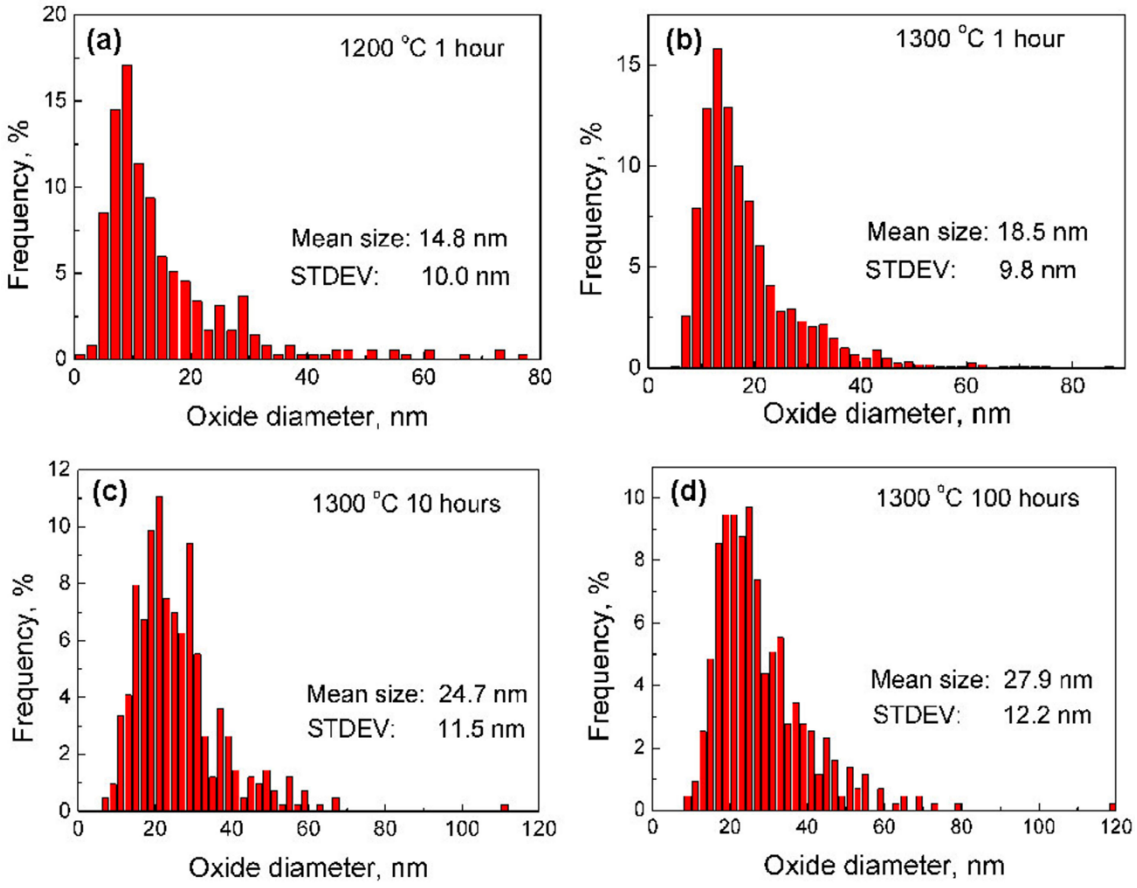

Figure 8. Size distribution of the oxide nanoparticles in PM2000 after annealing at (a) 1200 °C for 1 hour, (b) 1300 °C for 1 hour , (c) 1300 °C for 10 hours, and (d) 1300 °C for 100 hours. Measurements were conducted in TEM thin foils, and Feret diameters of at least 1000 particles were determined for each sample.

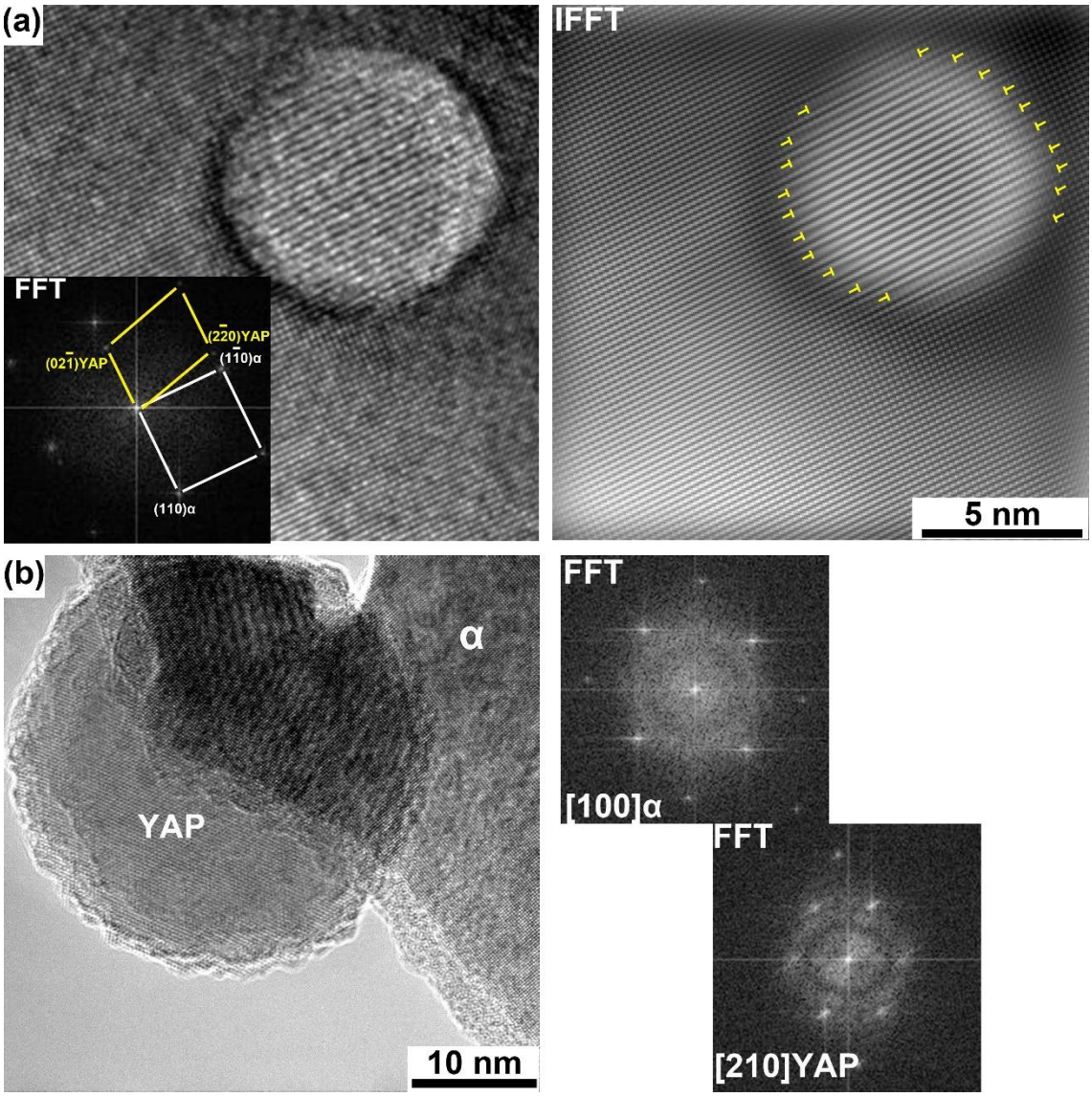

Figure 9. HRTEM images and corresponding FFT patterns and IFFT images of two oxide particles in PM2000 after annealing at 1200 °C for 1 hour. (a) HRTEM image and FFT pattern of a YAP particle with ferrite matrix; an IFFT image after filtering the noise is shown on the right hand side, in which misfit dislocations around the interface are marked by yellow symbols. (b) HRTEM image and FFT pattern of a YAP particle with the ferrite matrix and their separated FFT patterns.

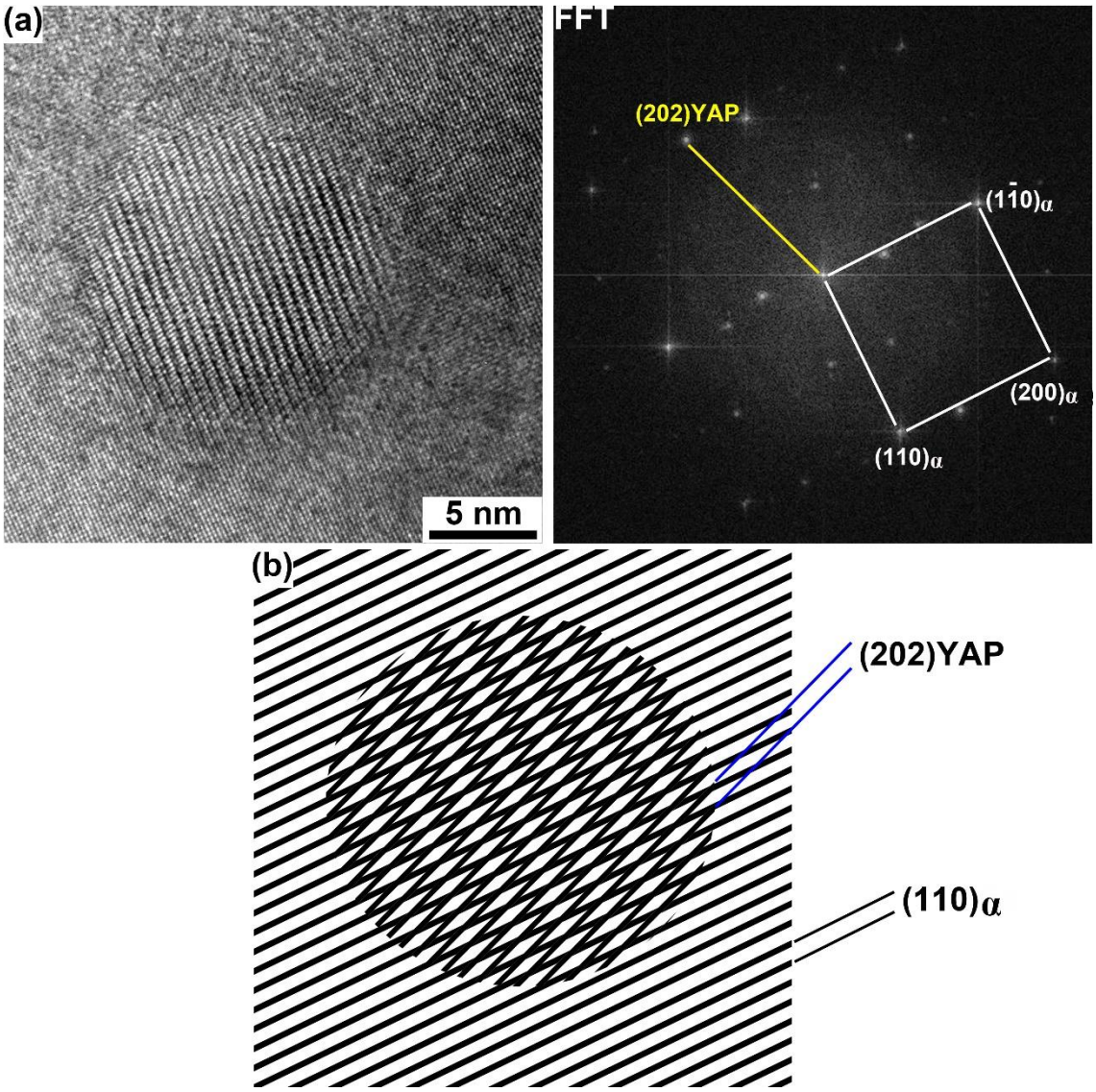

Figure 10. (a) An HRTEM image and the corresponding FFT pattern of a YAP nanoparticle in PM2000, which has an incoherent interface with the matrix, after annealing at 1200 °C for 1 hour. Moiré fringes appear on the interface of ferrite matrix and YAP. (b) Simulated Moiré fringes from two superimposed sets of parallel gratings, corresponding to the planes of $(110)_{\alpha}$ and $(202)_{YAP}$ with a relative rotation of 19.1° between them.

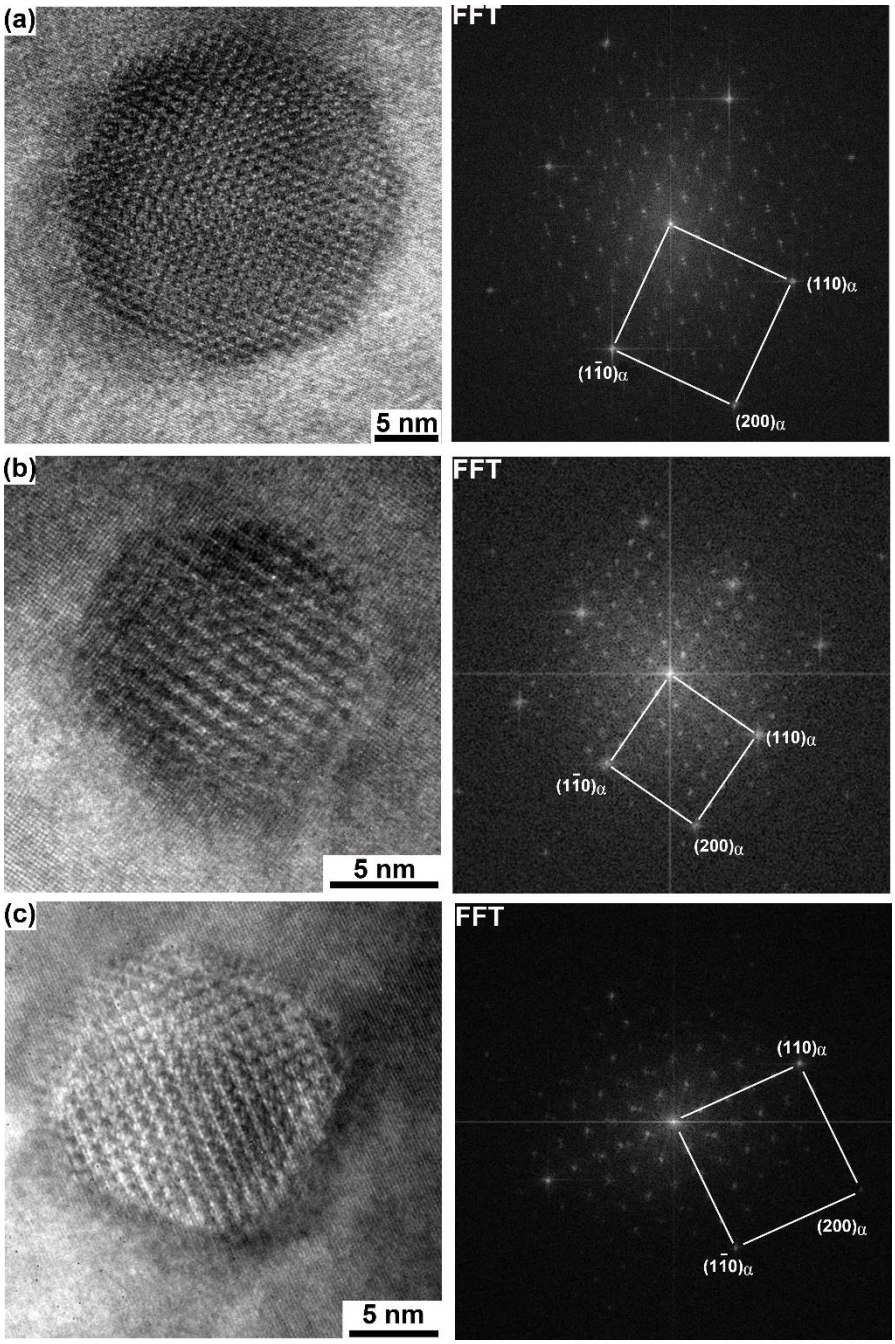

Figure 11. HRTEM images of three YAP nanoparticles in PM2000 after annealing at 1300 °C for 10 hours. The diffraction patterns from the ferrite matrix are indexed in the corresponding FFT patterns. The incident electron beam is along the $[001]_{\alpha}$ and $[010]_{YAP}$.

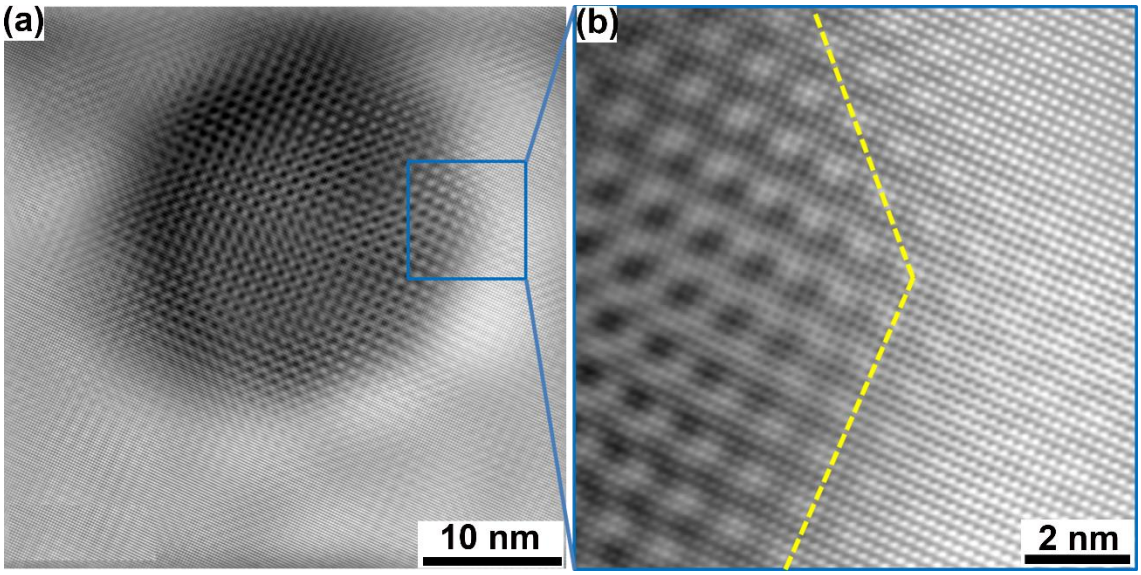

Figure 12. (a) An IFFT image of the HRTEM image in Fig.11a, after a filtering process to reveal the ferrite matrix and double diffraction products of superimposed ferrite and a YAP particle, (b) more detailed image from the framed region in (a), with yellow dashed lines between the ferrite matrix and YAP particle.

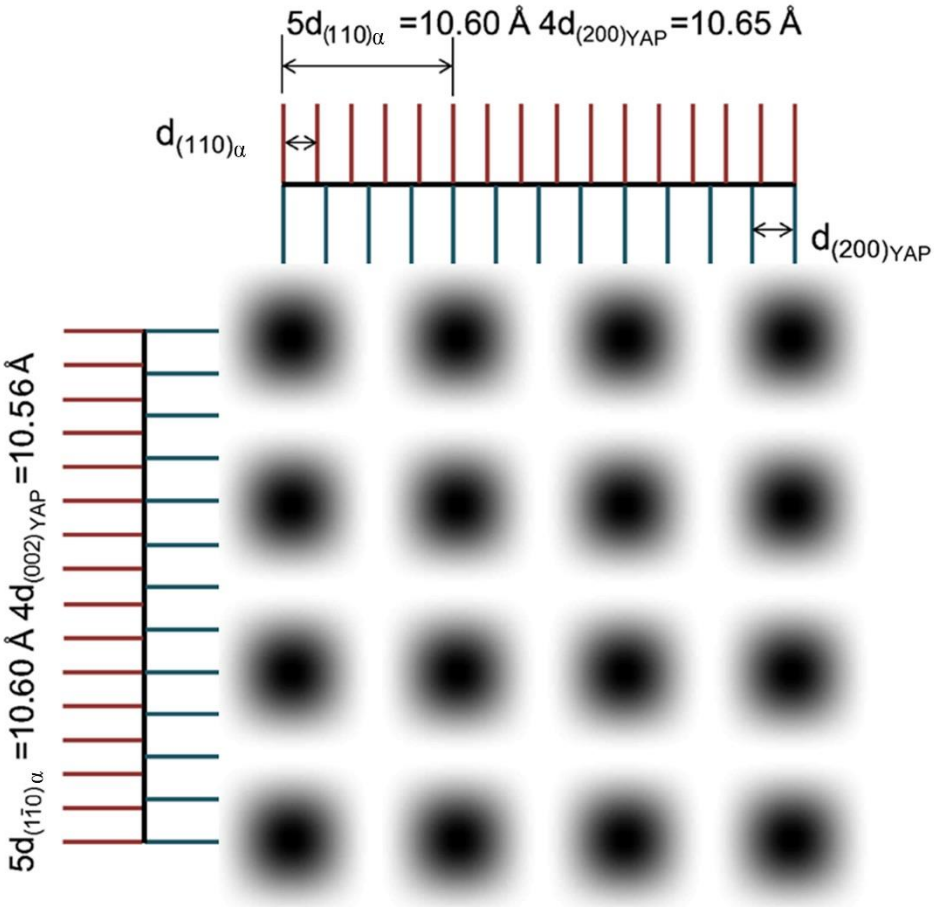

Figure 13. Sketch illustrating the origin of the Moiré patterns observed in Fig. 12. Four sets of gratings, representing $(110)_{\alpha}$, $(200)_{YAP}$, $(1\bar{1}0)_{\alpha}$, and $(002)_{YAP}$ are superimposed in a way that $(110)_{\alpha}||(200)_{YAP}$, and $(1\bar{1}0)_{\alpha}||(002)_{YAP}$. The viewing direction is along $[010]_{YAP}$ and $[001]_{\alpha}$.

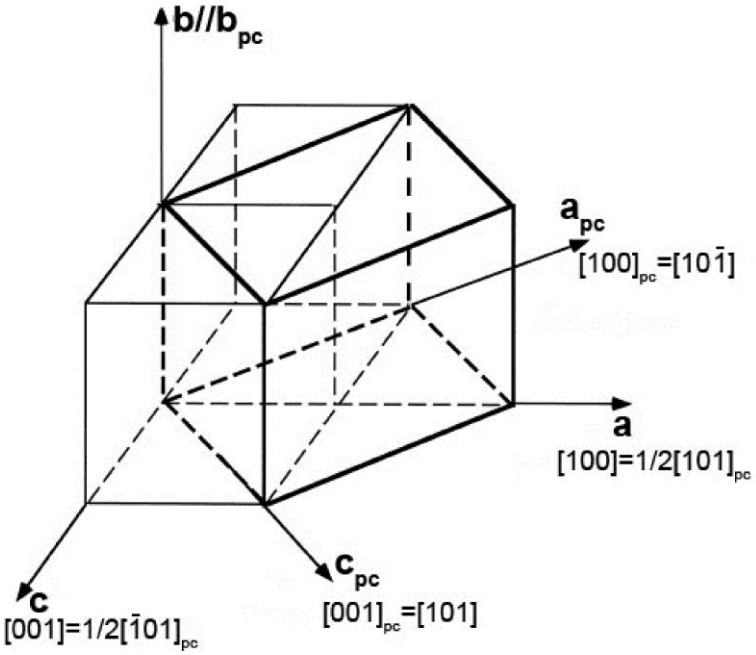

Figure 14. Sketch of two orthorhombic primitive crystal unit cells of YAP (two cuboids with thin lines) and the unit cell of the pseudo-cubic (pc) lattice (cube with thick lines).

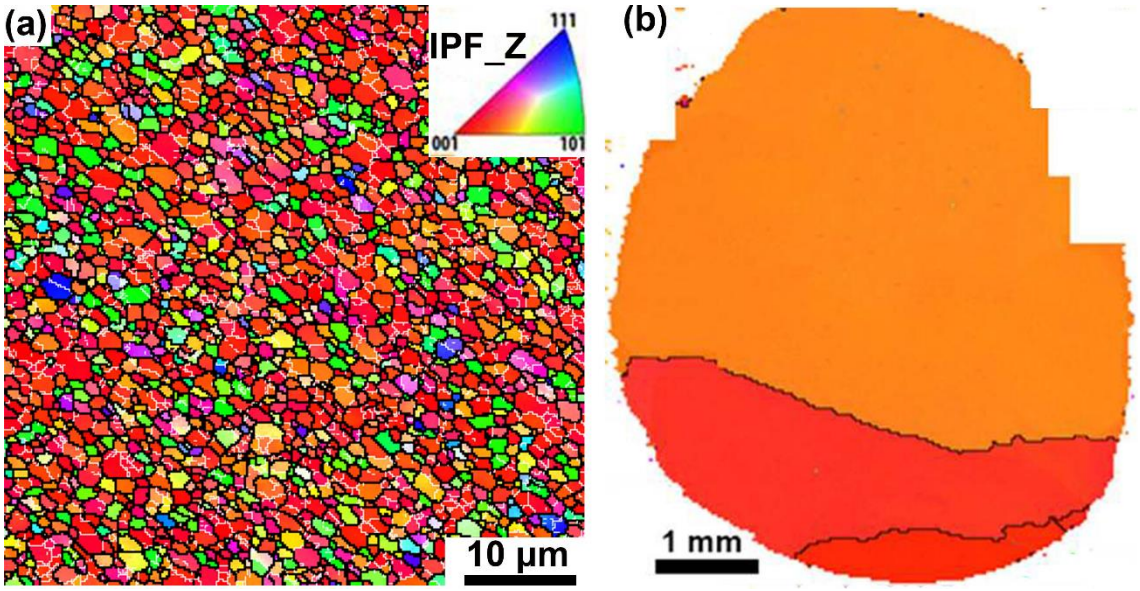

Figure 15. Orientation maps obtained by EBSD of PM2000 in cross section of (a) as-received material and (b) after annealing at 1200 °C for 1 hour. Different colors in the maps correspond to different crystallographic directions along the extrusion direction as shown in the inset. Black and white lines represent boundaries with misorientation angles higher and lower than 15°, respectively.

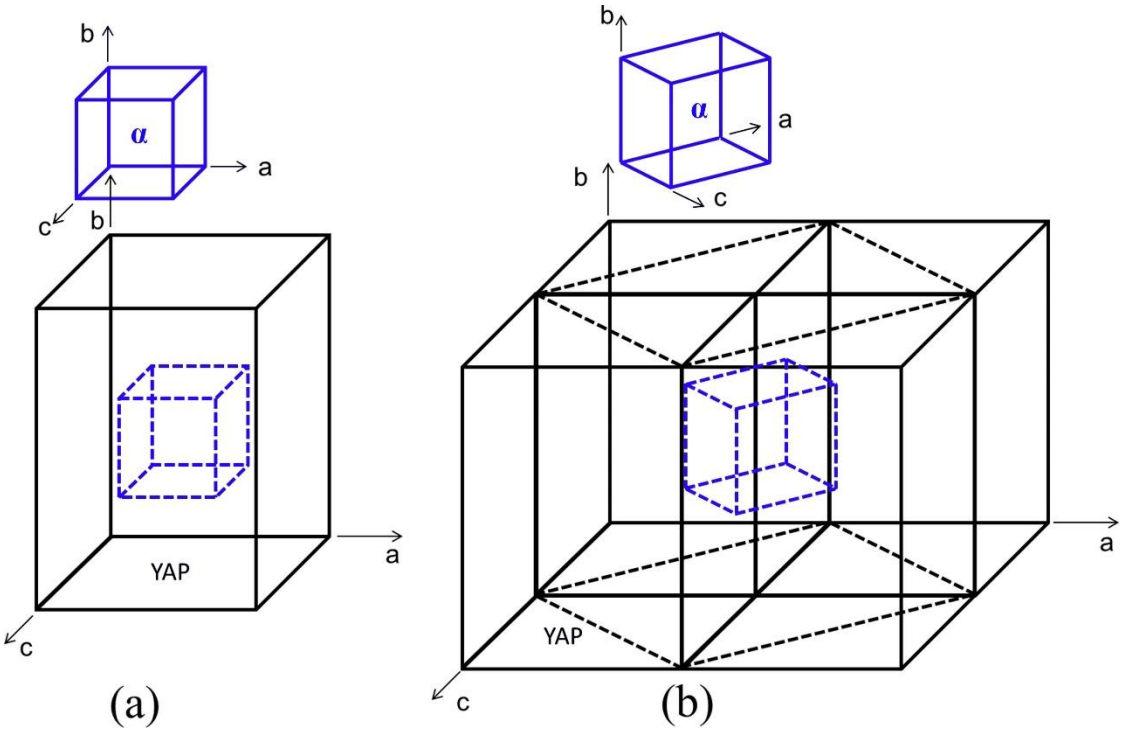

Figure 16. Schematic diagrams comparing the observed orientation relationships between YAP and ferrite: (a) Primitive unit cells of ferrite and YAP, showing the cuboid-on-cube orientation relationship between YAP and ferrite in the as-received sample, and (b) unit cell of ferrite and four unit cells of YAP illustrating the new pseudo cube-on-cube orientation relationship that developed in the sample after annealing at 1300 °C for 10 hours. The black dashed lines in (b) represent the unit cell of the pseudo-cubic lattice. The blue dashed lines represent an overlain ferrite unit cell.